CHAPTER 5

SOURCE POSITIONS, OBSERVATIONS AND RESULTS

5.1 AIM OF THE OBSERVATIONS

From many studies of radio recombination lines over a wide range of frequencies from 86GHz to 26MHz, it has now become known that there is a whole hieararchy of ionized regions with different densities, temperatures and sizes distributed in different ways in the galaxy. The properties of these different components of the ionized gas are however not well understood. The present observations were aimed at an understanding of the properties and distribution of low density ionized gas present in the galactic plane.

As discussed in chapter 2, in a heterogeneous medium low frequency recombination lines (viz. at <1GHz) preferentially sample conditions in low density ionized gas present along the line of sight. At these frequencies, recombination lines from higher density gas are suppressed due to the effects of pressure broadening, optical depth and beam dilution. On the other hand, the lines from low density gas are enhanced due to stimulated emission in the presence of strong background sources or even the non-thermal galactic background. Further, for large low density regions, beam dilution due to the poorer angular resolutions available at low frequencies is also less severe. Frequencies below 500MHz are best suited to study conditions in cold partially ionized gas. Calculations by Shaver (1975) have shown that stimulated emission of recombination lines at low frequencies due to the presence of a strong background source is most important for cold ionized regions. As mentioned before, it is at these frequencies that the nonthermal sources and the galactic background are most intense. The present observations can therefore detect recombination lines from cold HI gas if the ionization is adequate in these regions. Non detection would of course imply upper limits to the ionization rates in these clouds. Such limits are important for the theories that try to explain the overall nature of the interstellar medium (e.g. Field et al 1971, Mckee and Ostriker 1977).

Most existing large scale recombination line surveys of the galaxy have been carried out at frequencies higher than 1GHz (see Wilson 1980 and references therein). Below 500MHz, there are only a handful of observations made towards a few selected sources in the galactic plane (see Pedlar and Davies 1980 and references therein). Weak recombination lines have been detected at centimetric wavelengths at several positions along the galactic ridge (Gottesman and Gordon, 1970, Gordon and Cato 1972, Jackson and Kerr 1975, Mathews et al 1973, Lockman 1976, Hart and Pedlar 1976). These lines were initially thought to be coming from cold partially ionized clouds in the ISM (Gordon and Gottesman 1971) but are now believed to be due to low density hot gas presumably weak HII regions (Jackson and Kerr 1975, Hart and Pedlar 1976, Shaver 1976, Lockman 1980). However, the properties of this gas are not well understood. There are no comparable observations at frequencies below 500MHz to help understand these galactic ridge recombination lines. The only attempt at a large scale survey of these lines at 408MHz (Batty 1976) along the galactic ridge was done with very low sensitivity and consequently did not detect any lines.

The recombination lines reported in this thesis constitute the first major survey of the galactic plane below 1GHz. The data obtained can yield the distribution, kinematics and thermodynamic properties of low density ionized gas in the galactic plane. It is possible to get quantitative estimates of the amount of stimulated emission due to the presence of strong background sources. Such estimates would be important in assessing the feasibility of recombination line observations towards distant extragalactic sources. The present observations can also provide meaningful constraints on the properties of the distributed ionized gas in the general interstellar medium

5.2 OBSERVING FREQUENCY:

The rest frequency of the H272 recombination line calculated using the Rydberg formula is 324.9915MHz. The value of the frequency alone can put constraints on the density and emission measure of the ionized gas sampled by these observations.

The continuum optical depth of the ionized gas is approximately given by

$$\tau_c = 8.236 \times 10^{-2} \cdot \nu^{-2.1} \; T_e^{-1.35} \; E_c \qquad (5.1)$$

where ν is the frequency in GHz, T is the electron temperature (°K) and E_c is the emission measure given by

$$E_c = \int_0^L N_e^2 \, dl$$

N_e is the electron density and L is the path length through the gas.

If the optical depth exceeds unity, then the recombination lines tend to merge with the continuum This happens at the H272α frequency when

$$E_c \gtrsim 1.15 \times T_e^{1.35} \; pc \; cm^{-6}$$

For an electron temperature of 8000k and path length of 100pc this condition is satisfied for $N_e > 50cm^{-3}$.

The width of the recombination lines due to pressure broadening alone (Brocklehurst and Leeman 1971) is given by

$$\Delta\nu_{Lp} = 3.74 \times 10^{-11} \cdot Ne \cdot Te^{-0.1} \cdot n^{4.4} \; KHZ$$

where n is the principal quantum number. This broadening removes the energy in the line centre and spreads it into the Lorentzian wings of the profile making the line very weak. For n = 272 this width exceeds 100KHz for $N_e > 120cm^{-3}$. When the lines are broad and weak they become virtually undetectable.

A majority of the HII regions which are prominent in most radio continuum surveys (eg. Shaver and Goss 1970, Altenhoff 1978) have densities higher than $100cm^{-3}$ and sizes less than 10 arcminutes. Therefore, the recombination lines from these sources, in addition to being weaker due to optical depth and pressure broadening effects are further reduced in intensity due to beam dilution. As the ORT has a beam size of $2^\circ \times 6'$ the dilution factor is typically 10–50.

It therefore appears that observations at this frequency can only detect lines from large low density ionized regions. The nonthermal galactic background at 325MHz has a brightness temperature of 600–700K in the galactic plane. This can enhance the recombination line intensities due to stimulated emission in low density regions.

5.3 SOURCE POSITIONS:

The source positions for these observations were selected from the galactic plane continuum surveys of Shaver and Goss(1970a) and Altenhoff et al (1978). Most of the positions selected are in the first quadrant of the galaxy. The galactic longitude is restricted to $\ell < 60^\circ$ due to the limited declination coverage of the Ooty radio telescope ($-30^\circ < \delta < 30^\circ$).

Due to the long integration times required for detecting recombination lines at this frequency, a complete coverage of all the sources in the plane would require an impractical amount of telescope time. For these observations, 53 directions were selected to lie at somewhat coarser angular intervals but also so as to provide a variety of physical conditions in which to study recombination lines.

All the positions selected in the first quadrant of the galaxy are shown in figure 5.1. In addition, 3 more directions lying in the anticentre direction were also selected for observtion. The typical distribution of sources in the galactic plane can be seen in figures 5. 2a and 5. 2b reproduced from the survey of Altenhoff et al (1978). The ORT beam is superposed on these maps to'indicate the typical observed source positions.

The 53 directions selected for observations in our survey can be classified into 4 groups

1. HII REGIONS : 34 directions corresponding to HII regions of different densities and temperatures as determined by high frequency studies (e. g. Shaver and Goss 1970). For reasons discussed above, the higher density HII regions are unlikely to produce detectable recombination lines at these frequencies. However these observations can sample conditions in either low density outer envelopes of these HII regions, or low density ionized gas present along the line of sight'. 3 of the HII regions are in the anticentre direction where the intensity of the nonthermal galactic background is considerably less.

2. SUPERNOVA REMNANTS : 12 directions correspond to well known strong SNRs in the galactic plane. These directions are particularly suited for studying the effect of stimulated emission at low frequencies due to the strong background continuum source. There is ample evidence for the existence of substantial amounts of ionized gas along the line of sight to these sources. Most of these sources have shown a turn over in their continuum spectra at low frequencies (Dulk and Slee 1972,1975) which is attributed to free-free absorption by ionized gas along the line of sight. In addition, high frequency recombination lines have been detected towards a few of these sources (eg. Downes and Wilson 1974)

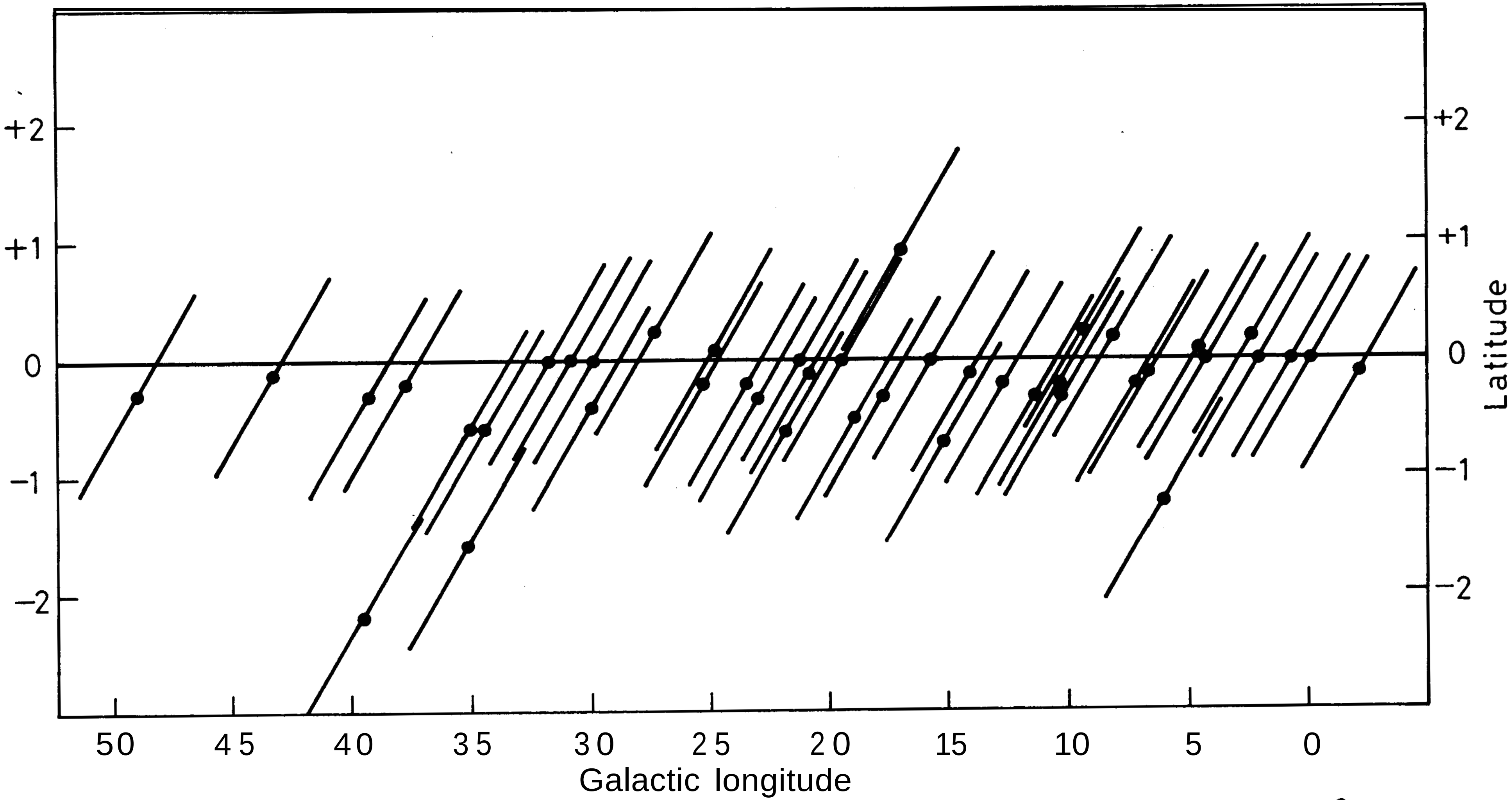

Fig. 5.1 The positions observed for 272α lines in the longitude range 0° to 50°. The dots indicate the centre of the ORT beam. The length of the inclined lines correspond to the 2° east-west beam of ORT.

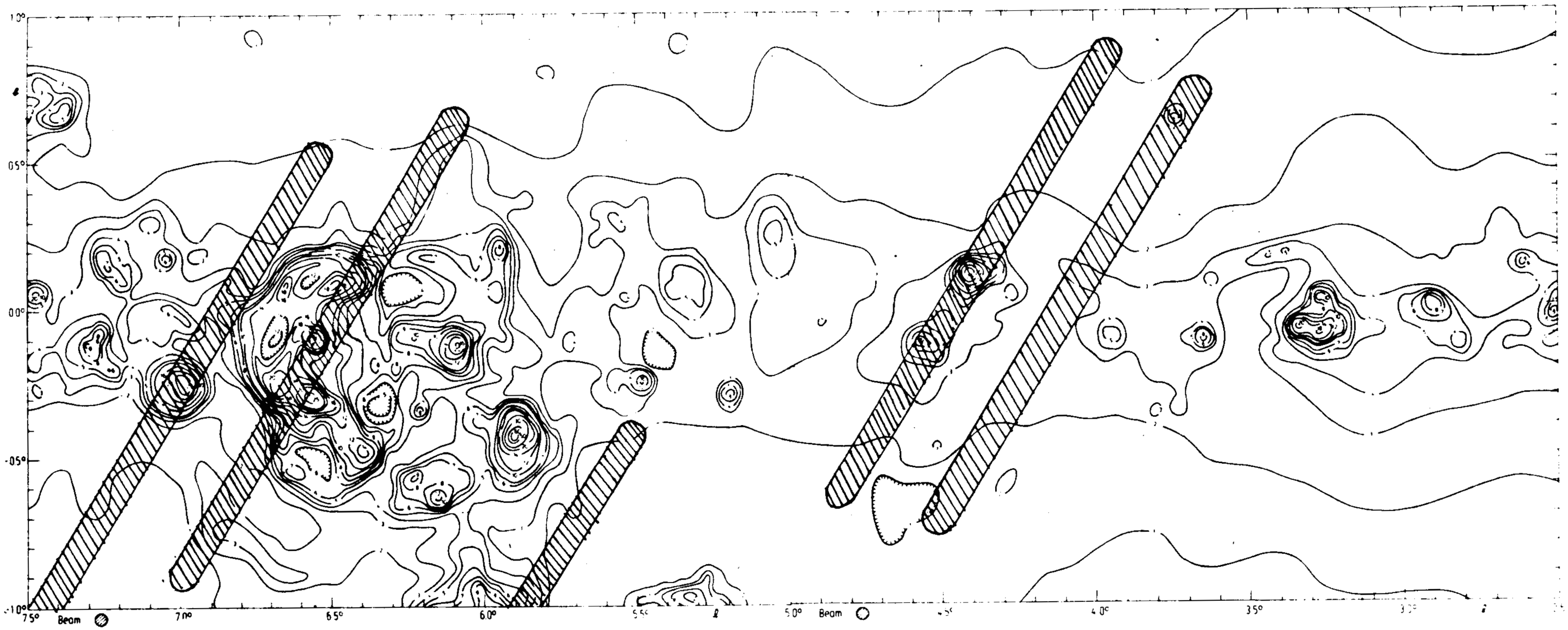

Fig. 5.2a ORT beam positions used in the longitude range 2°.5 to 7°.5 superposed on the 5 GHz continuum map of Altenhoff et. al. (1978). The hatched areas indicate the size and positions of the ORT beam.

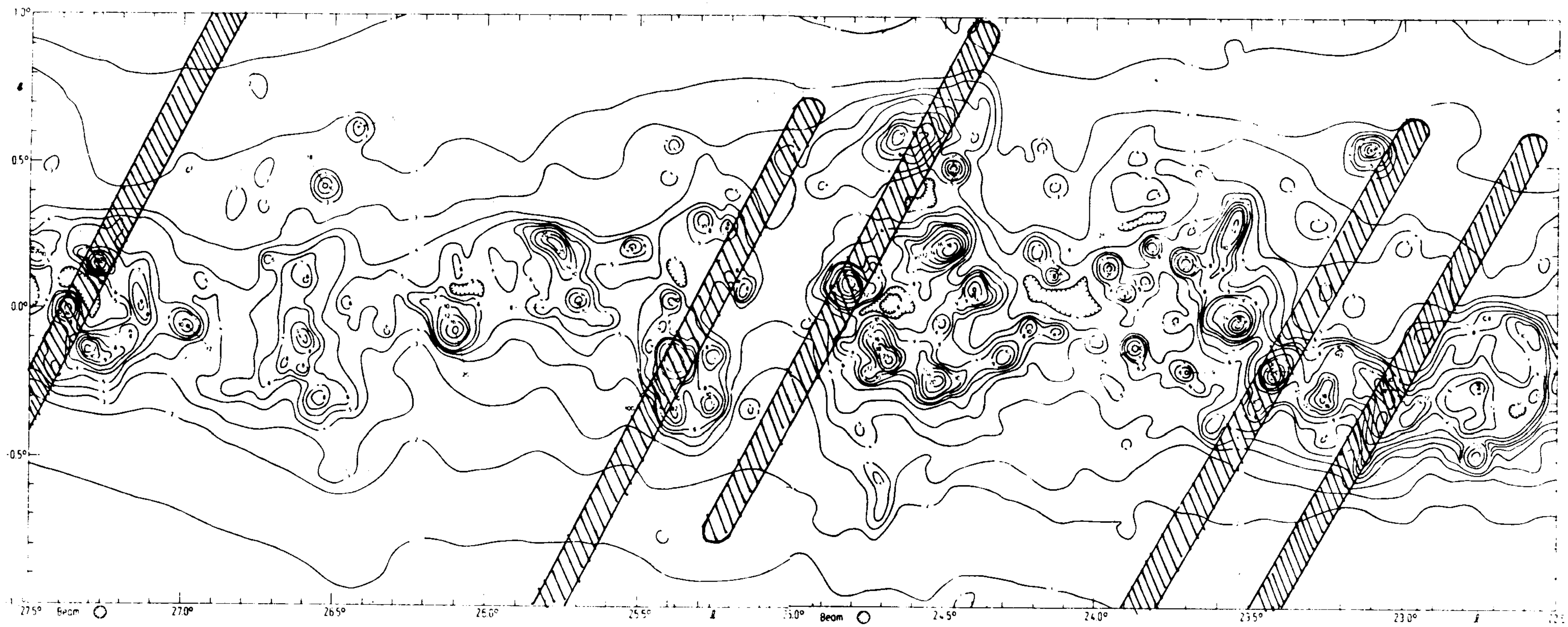

Fig. 5.2b Distribution of sources in the galactic plane in the 5 GHz survey of Altenhoff et. al. (1978). The hatched areas indicate some of the ORT beam positions in the present study.

3. BLANK REGIONS : The high resolution continuum map at 5GHz by Altenhoff et al (1978) was used to select six regions in the galactic plane devoid of any sources within the beam used for these observations. We call these directions 'blank regions'. Recombination lines at centrimetric wavelength have been detected towards several such directions in the galactic plane (eg. Gottesman and Gordon 1970, Lockman 1976, Mebold et al 1976). The observations at low frequencies can provide complementary information and help understand the origin of the galactic ridge recombination lines.

4. THE GALACTIC CENTRE : This is a unique direction towards which a variety of observations have been carried out by many workers. The direction has a strong background continuum source Sgr A and provides a long path length of 10kpc along the line of sight to this source. As differential galactic rotation does not contribute to broadening of the line, it is ideally suited for studying the integrated properties of the entire line of sight.

Table 5.1 gives all the observed source positions in galactic and equatorial coordinates. Well known names of the sources, where available, are indicated in column 4. The nature of the source is given in column 5.

5.4 OBSERVATIONS AND DATA REDUCTION

The observations were made in several sessions during the period from August 1980 to May 1982 using the 128 channel one-bit autocorrelator described in chapter 3. During this period the ORT was undergoing several modifications. For example, the feed system was being changed from the old mechanical phase shifters to the new diode phase shifters; the front end RF amplifier and mixer were being changed; filters to reject the ORT image band were being installed. As a result some of these observations

TABLE 5.1 : Source Positions and Continuum Temperatures

Galactic l	b	RA(1950) h m s	DEC(1950) ° ' "	Source name	Source type	Telescope configu-ration[L]	Total Continuum Temp(K)[1]
1		2	3	4	5	6	7
357.7	-0.1	17 36 57	-30 56 41	......	SNR	A	930
359.9	-0.0	17 42 27	-28 59 04	SGRA	G. CENTRE	A	2330
0.7	-0.0	17 44 10	-28 21 59	SGR B2	HII	A	1100
2.1	-0.0	17 47 27	-27 07 29	......	BLANK	B	740
2.3	+0.2	17 46 56	-26 49 35	......	HII	B	750
4.2	-0.0	17 52 14	-25 18 49	......	BLANK	B	690
4.4	+0.1	17 52 13	-25 04 52	AMW35	HII	A	700
6.0	-1.2	18 00 33	-24 23 25	M8	HII	D	660
6.6	-0.1	17 57 54	-23 21 17	U28	SNR	D	900
7.0	-0.3	17 59 17	-23 02 54	M20	HII	A	720
8.1	+0.2	17 59 55	-21 48 17	......	HII	A	770
9.4	+0.1	18 03 03	-20 45 22	......	BLANK	C	730
10.2	-0.3	18 06 25	-20 19 42	W31	HII	D	610
10.3	-0.2	18 05 60	-20 05 52	......	HII	B	680
11.2	-0.3	18 08 31	-19 26 31	......	SNR	A	760
12.8	-0.2	18 11 10	-17 57 56	W33	HII	A	730
14.0	-0.1	18 13 26	-16 51 55	......	HII	A	680
15.1	-0.7	18 17 35	-16 12 22	M17	HII	D	810
15.7	-0.0	18 16 24	-15 17 58	......	BLANK	C	610
16.9	+0.7	18 16 08	-13 51 41	M16	HII	C	610
17.6	-0.3	18 21 17	-13 44 04	......	BLANK	C	630
18.9	-0.5	18 24 21	-12 44 28	......	HII	A	660
19.6	+0.0	18 23 56	-11 52 40	......	HII	D	550
20.7	-0.1	18 26 26	-10 54 53	......	HII	A	590
21.2	-0.0	18 27 01	-10 28 09	......	BLANK	B	580
21.8	-0.6	18 30 25	-10 12 46	......	SNR	A	790
23.0	-0.3	18 31 27	-08 57 27	W41	SNR	A	770
23.4	-0.2	18 31 57	-08 35 51	......	HII	A	750
24.8	+0.1	18 33 29	-07 13 10	......	HII	A	660
25.4	-0.2	18 35 31	-06 50 32	3C385	HII	A	650
27.3	+0.2	18 37 53	-05 00 47	......	HII	A	640
28.8	+3.5	18 28 48	-02 07 37	W40	HII	A	450
29.9	+0.0	18 43 30	-02 44 01	......	HII	B	650
29.9	-0.2	18 43 25	-02 43 47	......	HII	A	680
30.8	+0.0	18 44 50	-01 59 04	W43	HII	C	830
31.9	+0.0	18 46 51	-00 58 52	3C391	SNR	A	680
34.6	-0.6	18 53 57	+01 06 20	W44	SNR	A	830
34.7	-0.6	18 54 13	+01 14 24	W44	SNR	A	950
35.1	-1.6	18 58 43	+01 08 24	W48	HII	A	460
37.8	-0.2	18 58 30	+04 09 54	W47	HII	D	480
39.2	-0.3	19 01 35	+05 21 35	36396	SNR	A	570
39.7	-2.2	19 09 21	+04 53 48	W50	SNR	B	360

..... continued

Table 5.1 : continued.. ...

1		2	3	4	5	6	7
43.2	-0.1	19 08 16	+08 59 54	W49	SNR	A	690
45.4	+0.1	19 11 57	+11 03 41	......	HII	B	360
49.0	-0.3	19 20 17	+14 02 01	W51B	HII	A	650
49.0	-0.6	19 21 23	+13 51 51	W51C	SNR	D	490
49.5	-0.4	19 21 27	+14 24 22	W51A	HII	A	450
51.4	+0.0	19 23 42	+16 14 17	......	HII	A	290
54.1	-0.1	19 29 27	+18 35 52	......	HII	A	210
59.8	+0.2	19 40 24	+23 42 32	......	HII	A	120
206.0	-2.1	06 28 29	+05 13 25	W16	HII	A	100
206.8	-16.4	05 39 11	-01 55 50	NGC2024	HII	A	120
209.2	-19.4	05 32 50	-05 25 09	ORION A	HII	A	420

Notes to TABLE 5.1:

1. Total beam averaged brightness temperature. Error on the measurement of this quantity is estimated to be ~15%.

   The 530m x 30m Ooty Radio Telescope is divided in to 22 equal modules along the north-south direction. Starting from the middle the northern modules are designated as N1, N2...N11 and southern modules as S1, S2...S11. Signals from each of the modules are brought independently into the receiver room and combined with proper phases and delays to form the final beam There is provision to switch off any of the modules thereby cutting off their contribution to the final output. These observations were made during the period when the telescope was undergoing major modifications. Therefore many sources in this list were observed with one or more modules switched off. Switching off modules starting from either end reduces the collecting area and broadens the beam Switching off intermediate modules creates a hole in the aperture, reducing the collecting area and introducting low level side lobes. For the purpose of this table the designation in this column mean the following A - All modules on, B - N1 module off, C - N1 and N2 modules off and D - .Modules S6 to S11 off.

have been made when parts of the telescope were not functioning, and sometimes with a different sensitivity. Column 6 of Table 5.1 indicates the configuration of the telescope used for different observations. However, during all the observing sessions, the line intensities were measured with respect to the adjoining continuum, which to first order removes the dependence on system parameters.

A bandwidth of 500KHz, corresponding to a velocity coverage of $\sim$461km/s at the H272α frequency, was used during all the observations. This bandwidth can cover both the hydrogen and carbon recombination lines which are separated by about 150KHz. After Hanning smoothing of the autocorrelation function, the spectrometer gives a velocity resolution of 7.2km/s.

The observing proceedure was as outlined in section 4.5. Double frequency switching was used for all the observations. Each source was observed on 3 to 4 days, either on succesive days or separated by several days depending on the availability of telescope time. Interspersed observations of different sources is desirable as it makes it easier to check for the presence of interference. The setting of the first local oscillator frequency on any day was decided by the expected velocity of the recomibination line in the direction of observation. The online frequency was chosen such that the expected hydrogen and carbon recombination lines fell within the observing band of 500KHz.

Data was acquired in stretches of 1 to 1.5 hours (referred to as a SCAN) while tracking the source position over an hour angle range generally between -4^h to 4^h30^m. All the data acquired was written onto magnetic tapes after averaging for 1 minute during the acquisition. The data recorded on magnetic tapes were processed using the data reduction methods described in section 4.6. All the sepctra were calibrated in units of line to total continuum ratio (equation 4.9)

For some of the sources, the data was further smoothed to improve the signal to noise ratio. It was ensured that the smoothing process did not affect any narrow features by comparing the unsmoothed and the smoothed spectra. Gaussians were fitted to the line profiles using a standard least squares technique and the line parameters were determined. For each source the residuals obtained after subtracting the gaussian components from the final spectrum was examined. In all the cases the residuals showed rms noise fluctuations consistent with that expected for a one-bit autocorrelator as given by eqn 3.13.

For each of the gaussian line components fitted to the final spectrum one obtains 3 parameters. These are

1. Peak amplitude A (in units of T_{BL}/T_{BS})
2. The centroid . V_0 (in km/s)
3. The full width at half maximum ΔV (in km/s)

The formal statistical errors on each of these parameters can be computed from the rms noise on the residuals. If the signal being analysed has gaussian statistics as is true for most of the radio astronomical signals, then the rms errors on each of the above parameters is given by (see Rieu 1969)

$$\sigma_A = \left(\frac{\Delta V_0}{\Delta V}\right)^{1/2} \sigma_r$$

$$\sigma_{\Delta V} = 1.16\,(\Delta V_0 \times \Delta V)\,\frac{\sigma_r}{A}$$

$$\sigma_{V_0} = 0.49\,(\Delta V_0 \times \Delta V)^{1/2}\,\frac{\sigma_r}{A}$$

where σ_r is the rms noise of the residuals and ΔV_0 is the instrumental resolution. These equations were used to compute the errors on each of the parameters for all the sources.

The source G359.9-0.1 (SgrA) was observed several times during the one and half year period of these observations to ensure the satisfactory functioning of the system at all times. This has resulted in a particularly long integration time and therefore the best signal to noise ratio for this source.

Continuum measurements of all the sources observed for recombination lines were made in a separate session in April 83. Although the observed lines were already calibrated in terms of line to continuum ratios, these measurements were necessary for the interpretation of the line parameters in terms of the physical properties of the line emitting region; the total background continuum radiation can cause stimulated emission of these lines as discussed before.

The continuum temperature can be measured directly in brightness temperature units using the procedure described in section 4.4. For each of the sources in Table 5.1 this was done using the same configuration of the telescope as was used during the line observations (column 6 of Table 5.1). The increase in total system temperature was first measured for each source postion, with resepect to a cold region about 2.5 to 3 away in right ascension. This was compared with the increase in system temperature due to the sources 3C283 and HerA. The flux at 327MHz of 3C283 was taken to be 20.6 Jansky and that of HerA 200 Jansky. Necessary corrections were applied for the deviation of the total power detector law from a true square law. The comparison yielded an equivalent flux in the beam due to the source plus the background. This was converted to the average beam brightness temperature using the measured main beam solid angle of the ORT. No attempt was made to separate the contributions from the source in the beam and the background. The measured beam brightness temperature for each source is given in column 7 of Table 5.1.

5.5 RESULTS OF THE OBSERVATIONS :

Out of the 53 directions observed, recombination lines have been detected in 47 directions. The observed spectra in directions for which lines were detected are presented in Figures 5.3 to 5.6. Figure 5.7 shows the spectra in directions where no lines were detected. In figures 5.3 to 5.7, the ratio of line to total underlying continuum intensities have been plotted against radial velocity with respect to LSR, calculated using the rest frequency of the H272α recombination line. It should be stressed here that the continuum intensity in the above ratio is the total continuum intensity, including both the contribution

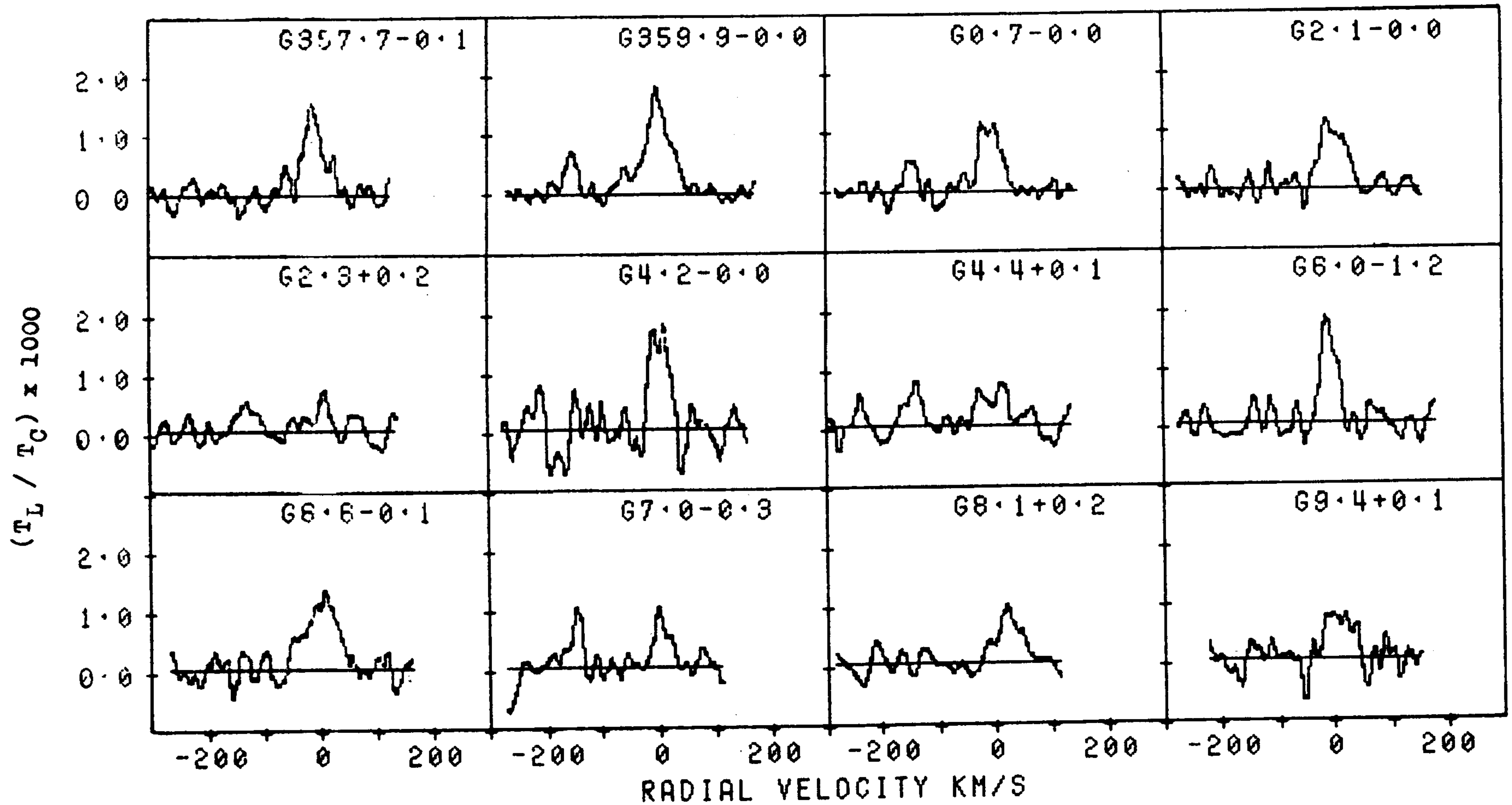

Fig. 5.3 The observed 272α spectra towards different sources. The T_c in the ordinate includes the galactic background.

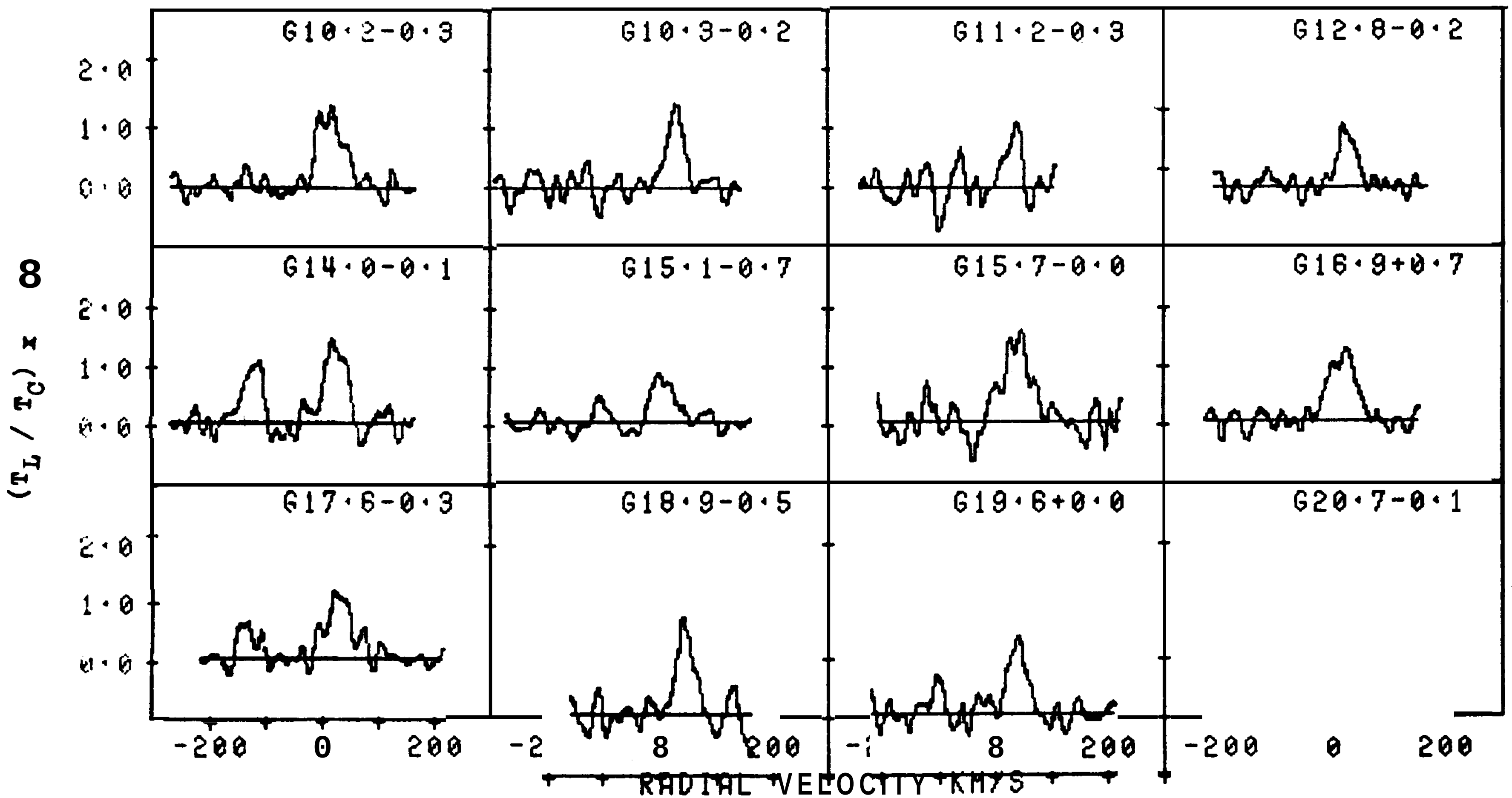

Fig. *5.4* Observed 272α spectra towards different sources. The continuum temperature in the ratio (T_L/T_C) includes the galactic background.

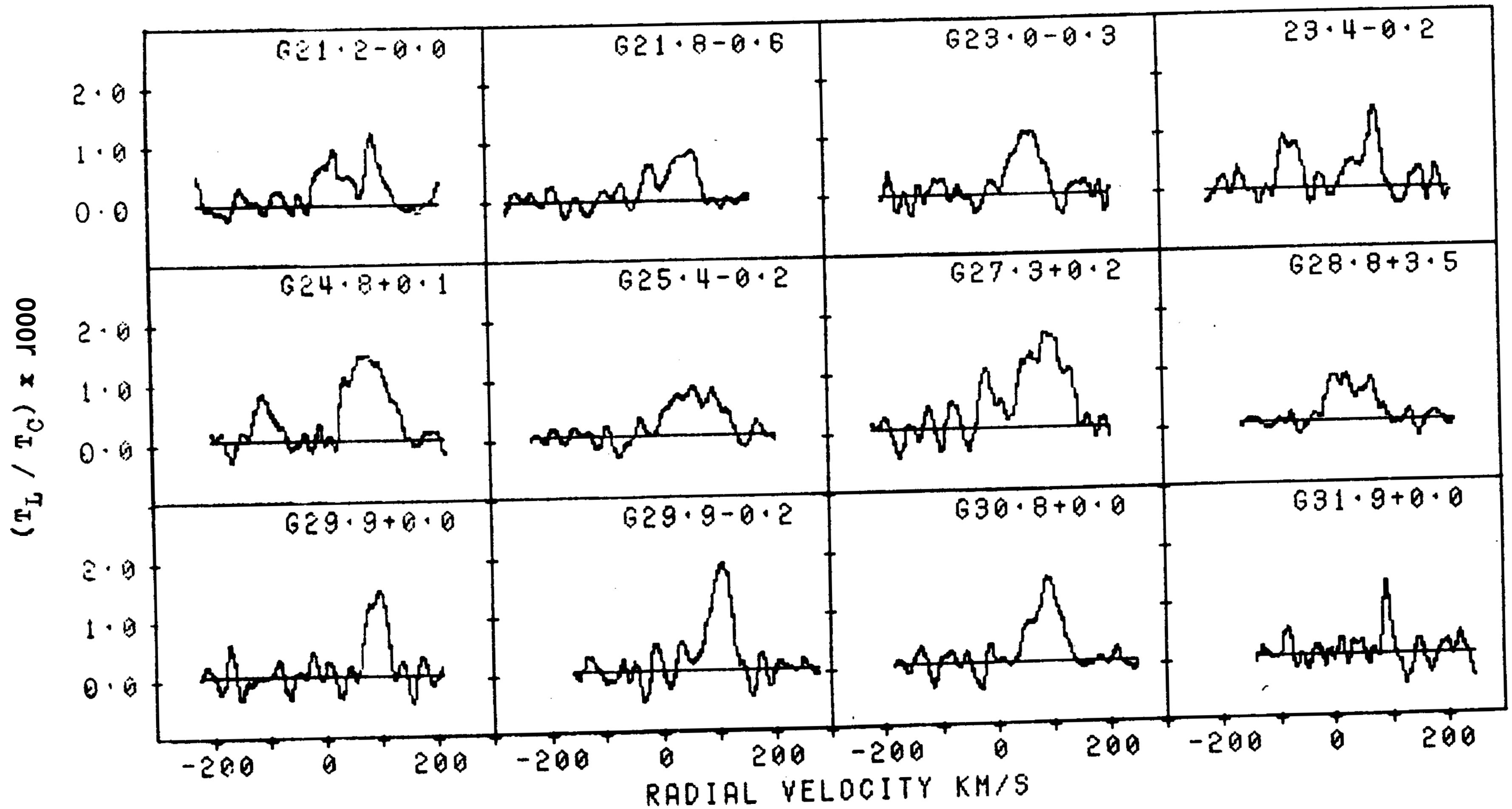

Fig. 5.5 The observed 272α spectra towards different sources. The T_c in the ordinate includes the galactic background.

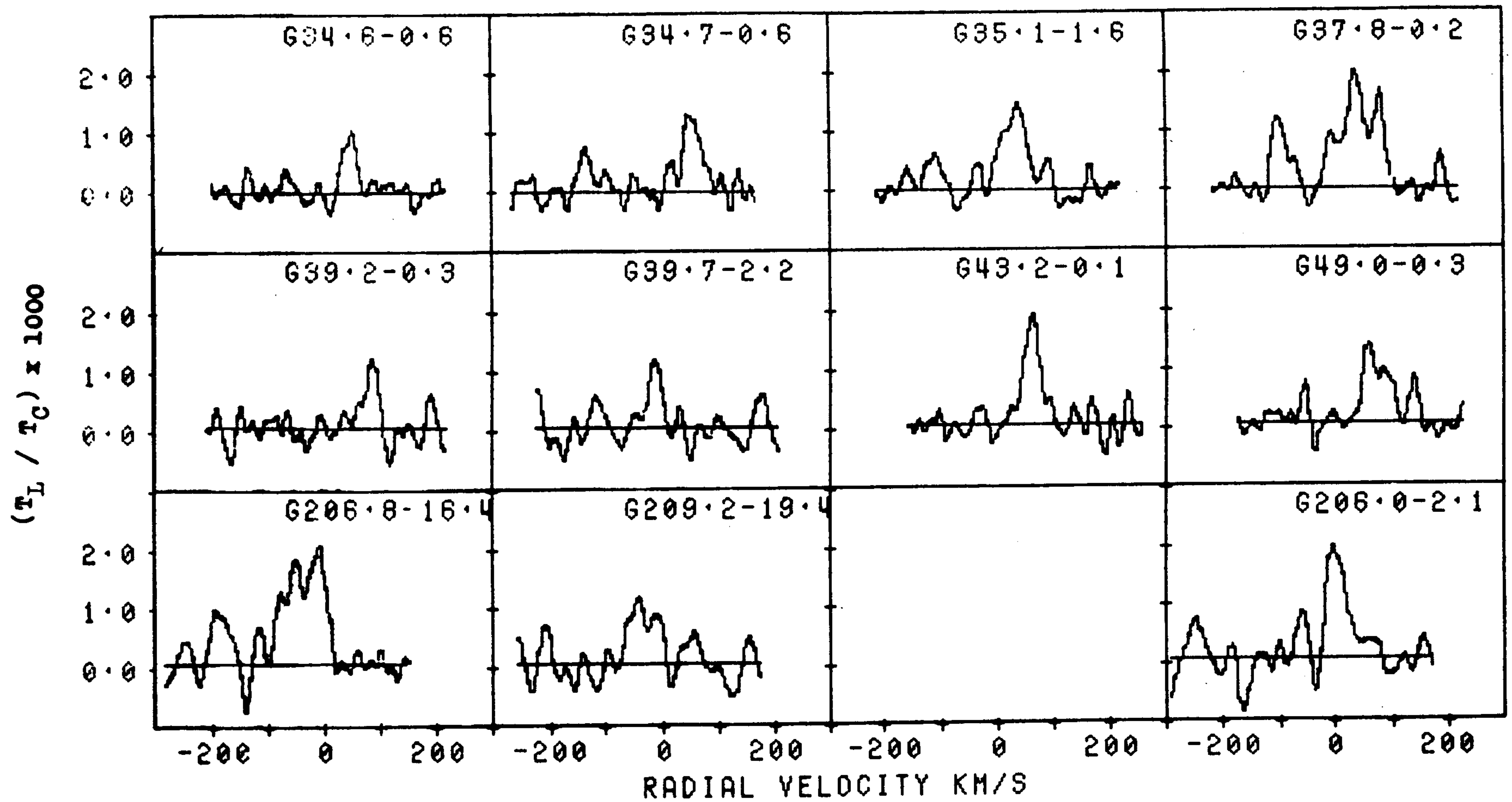

Fig. 5.6 Observed 272α spectra towards different sources. T_C includes the galactic background. The ordinate for the source G206.0 – 2.1 should be multiplied by 2.

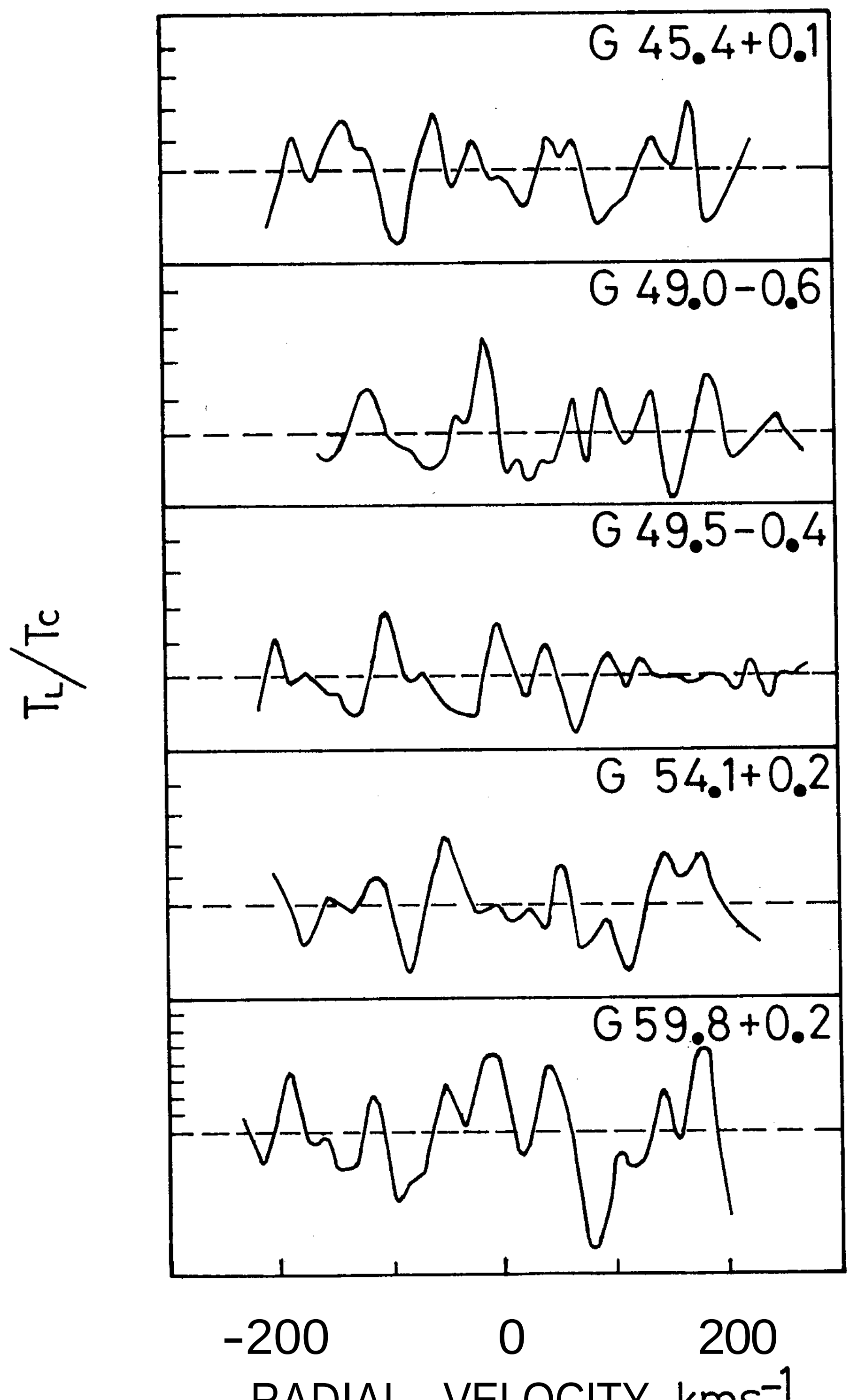

Fig. 5.7 Spectra towards sources where no line was detected. The marking on the ordinate correspond to $(T_L/T_C)=10^{-3}$. T_c is the total continuum temperature which includes the galactic background.

from the source and the nonthermal background. This is to be noted because in most of the high frequency radio recombination line surveys reported in the literature, the continuum intensity, used in the line to continuum ratios is only that due to the HII region.

The line parameters obtained from a least squares gaussian fit to the observed profiles, and the derived parameters are presented in Table 5.2. Column 2 to 4 of this table contain the peak amplitude, half power width and centroid of the fitted gaussian components. The line widths have been corrected for instrumental broadening. The errors quoted are one standard deviation derived from the rms noise of the residuals using equations 5.3. Columns 5 and 6 of this table give the velocity resolution of the spectra and the integration time respectively. The peak line brightness temperature T is given in column 7. This was obtained by multiplying the quantity in column 2 by the measured continuum beam brightness temperature for the source indicated in column 7 of Table 5.1. For many of the sources (particularly those with very wide lines), the individual line parameters obtained from the gaussian fit can only be used as indicators of the strength and extent of the line; a single gaussian component may not accurately represent the true line shape. However, the integrated line intensity computed from the gaussian parameters for each source is perhaps more meaningful and is given in column 8 of Table 5.2. Possible carbon lines have been excluded while obtaining this quantity.

The main results of this survey can be summarized as follows.

1. In the first quadrant of the galaxy, for longitude range $\ell < 40^\circ$ the hydrogen recombination line was detected towards every direction irrespective of whether it corresponds to an HII region, an SNR or a Blank region. Outside this range the line was detected only towards 2 strong sources, W49 and W51. The line was also detected towards the three HII regions in the anticentre

TABLE 5.2 : Observed Line Parameters and Integration times

Source	$H272\alpha$ Gaussian Parameters: Peak $T_L/T_c \times 10$	Width (FWHM) km/s	Velocity (LSR) km/s	Spectral Resolution km/s	Integration Time hours	Peak Line Temp T_{LB} (°K)	$\int T_{LB} d\nu$ K-KHz	Velocity of $H110\alpha$ [1] km/s	$V_{110\alpha} - V_{272\alpha}$ km/s
1	2	3	4	5	6	7	8	9	10
G357.7-0.1	1.39(09)	40(3)	-7.9(1.3)	10	25.9	1.3(2)	60(11)	....	.....
G359.9-0.0	0.59(04)	51(1.5)	4.7(0.6)	10	62.5	3.7(6) }	238(35)	18	13
	0.36(06)	21(4.5)	-57(2)			0.8(2) }			
	0.71(06)	24(2.5)	-149.5(1.0)*			1.7(3)	46(9)		
G0.7-0.0	1.1[illegible](06)	43(3)	-4.4(1.2)	12	22.9	1.24(20)	62(11)	64.6	69
	0.5[illegible](09)	20(4)	-146(2)*			0.64(14)	15(4)		
G2.1-0.0	1 10(07)	47(4)	5(2)	12	33.8	0 81(13)	44(8)	....	...
G2.3+0.2	0.64(13)	18(5)	9(2)	15	19.3	0.[illegible]8(12)	10(4)	5.0	-4
	0.48(10)	36(9)	-127(4)			0.36(09)	15(5)		
G4.2-0.0	1 9(2)	33(5)	7(2)	12	12.0	1 2[illegible](24)	49(11)	....	...
G4.4+0.1	0.56(09)	66(13)	4(5)	15	19.0	0.39(09)	30(9)	5.7	2
	0.70(13)	26(7)	-141(3)*			0.49(12)	15(5)		
G6.0-1.2	1.83(14)	26(3)	-4(1)	15	11.9	1.2(2)	36(7)	3.0	7
G6.6-0.1	1.2(1)	43(4)	11(2)	12	14.4	1.1(2) }	69(12)	12.5	2
	0.36(10)	41(13)	-27(6)			0.32(10) }			
G7.0-0.[illegible]	0.[illegible]7(13)	30(6)	6(2)	15	10.0	0.63(13)	22(6)	14.0	8
	1.[illegible](2)	14(4)	-144(2)			0.73(16)	12(4)		

..... continued

TABLE 5.2 : continued......

1	2	3	4	5	6	7	8	9	10
G8.1+0.2	0.83(09)	47(7)	25(3)	20	16.0	0.64(12)	35(8)	22	-3
G9.4+0.1	0.83(12)	42(7)	10(3)	12	24.6	0.61(13)	30(8)	.....	...
G10.2-0.3	1.27(08)	51(4)	15(2)	15	13.6	0.77(13)	45(8)	13.0	-2
G10.3-0.2	1.36(12)	29(3)	32(2)	15	12.0	0.92(16)	31(6)	12.0	-20
G11.2-0.3	1.1(2)	23(6)	37(2)	15	8.3	0.8(2)	22(7)	....	....
G12.8-0.2	1.0(1)	32(4)	26(2)	15	12.0	0.72(13)	27(6)	30.0	4
G14.0-0.1	1.4(1) 1.1(1)	38(3) 29(4)	24.1(1.5) -122(2)*	15	11.7	1.0(2) 0.74(14)	43(8) 25(6)	31.5	7
G15.1-0.7	0.83(07)	41(5)	9(2)	20	18.7	0.67(12)	32(7)	11.5(3)	
G15.7-0.0	1.4(1)	58(5)	43(2)	12	19	0.86(14)	58(11)	....	....
G16.9+0.7	1.19(06)	53(3)	20(1)	12	27.8	0.73(11)	45(7)	28.0	8
G17.6-0.3	1.07(08) 0.32(08)	47(4) 50(15)	30(2) -129(6)*	15	20.4	0.67(11) 0.20(06)	36(7) 12(5)	....	....
G18.9-0.5	1.6(2)	32(4)	48(2)	15	13.2	1.0(2)	38(9)	67	19
G19.6+0.0	1.3(1) 0.67(14)	35(3) 13(5)	41 (2) -100(2)*	15	16.7	0.71(12) 0.37(09)	29(6) 6(2)	55.3	14
G20.7-0.1	0.77(14)	19(6)	47(3)	20	9.9	0.45(11)	10(4)	57	10

.....continued

TABLE 5.2 : continued......

1	2	3	4	5	6	7	8	9	10
G21.2-0.0	1.11(10) 0.80(07)	26(3) 54(6)	98.6(1.3) 25(3)	15	20.5	0.64(11) 0.46(08)	48(7)	....	.....
G21.8-0.6	0.89(08) 0.62(12)	44(5) 13(5)	54(2) -9(2)	20	13.7	0.70(12) 0.49(12)	43(8)	.....	.....
G23.0-0.3	1.09(07)	55(4)	68(2)	12	18.7	0.84(14)	53(10)	78.0	10
G23.4-0.2	1.3(14) 0.93(13)	27(4) 30(6)	85(2) -64(2)*	15	14.5	1.0(2) 0.70(14)	31.(7) 24(7)	104.0	19
G24.8+0.1	1.51(06) 0.73(09)	77(4) 34(5)	83(2) -104(2)*	15	15.4	1.00(15) 0.48(09)	89(14) 19(5)	107.0	24
G25.4-0.2	0.78(06)	95(9)	64(4)	20	14.7	0.51(09)	56(11)	59.0	-5
G27.3+0.2	1.53(09) 1.0(2)	85(6) 18(5)	93(2) -12(2)	15	14.1	0.98(16) 0.65(15)	110(18)	33.0	-60 45
G28.8+3.5	0.61(06) 0.79(05)	35(4) 44(4)	72(2) 19(2)	15	17.5	0.27(05) 0.36(06)	29(4)	0.7*	-72 -19
G29.9+0.0	1.51(13)	35(4)	91(2)	15	13.0	1.0(2)	40(8)	98.5	8
G29.9-0.2	1.86(12)	37(3)	105(2)	15	21.8	1.26(21)	54(10)		
G30.8+0.0	1.42(08) 0.55(12)	41(3) 16(5)	95(1) 54(2)	15	20.5	1.2(2) 0.46(12)	64(11)	90.0	-5
G31.9+0.0	1.3(2)	10(2)	98(1)	12	22.2	0.9(2)	10(3)	103[+]	5

..... continued

TABLE 5.2 : continued......

1	2	3	4	5	6	7	8	9	10
G34.6-0.6	1.05(11)	21(3)	48(1)	12	13.0	0.87(16)	21(5)	53.0	5
G34.7-0.6	1.24(10) 0.69(13)	37(4) 20(5)	59(2) -132(2)*	12	14.3	1.2(2) 0.7(2)	50(10) 15(5)	50.3 [3]	-9
G35.1-1.6	1.33(12)	55(6)	34(3)	15	13.4	0.61(11)	39(8)	43.0	9
G37.8-0.2	1.59(11) 1.2(2)	81(6) 26(5)	48(3) -96(2)*	15	16.9	0.76(13) 0.57(12)	71(13) 17(5)	61.0	13
G39.2-0.3	1.15(14)	21(5)	84(2)	15	11.3	0.66(13)	16(5)	.....	.....
G39.7-2.2	1.1(2)	18(6)	-11(3)	20	17.5	0.4(1)	9(4)	.....	.....
G43.2-0.1	1.72(11)	35(3)	63(1)	12	28.1	1.2(2)	48(9)	10.0	-53
G45.4+0.1	<1.6	.....	.....	15	15.5	<0.6	....	54.5	.....
G49.0-0.3	1.1(1)	55(6)	75(3)	15	15.8	0.75(15)	46(10)	60.5	-14
G49.0-0.6	<1.3	.....	.....	15	11.3	<0.7	.....	....	.....
G49.5-0.4	<1.0	.....	.....	15	22.5	<0.5	.....	57.1	.....
G51.4+0.0	<2.1	.....	.....	20	11.0	<0.6	.....	53.3	.....
G54.1+0.2	<1.6	.....	.....	20	10.0	<0.3	.....	43.0	.....
G59.8+0.2	<4.0	....	.....	20	12.2	<0.8	.....	-6	.....

..... continued

TABLE 5.2 : continued......

1	2	3	4	5	6	7	8	9	10
G206-2.1	4.0(5)	28(5)	5(2)	20	32.3	0.4(1)	13(3)	7(3)[5]	2
G206.8-16.4	1.78(12)	84(7)	-36(3)	15	112.9	0.21(04)	20(4)	7.0[2]	43
	1.0(2)	26(7)	-187(3)*			0.12(03)	4(1)		
G209.2-19.4	1.0(2)	53(11)	-34(5)	20	23.2	0.43(10)	26(8)	-2.7[2]	31

Notes for Table 5.2 :

1. From Downes et al(1980)
2. Velocity of 10% line form Refenstein et al(1970)
3. Velocity of 166α line form Bignell(1973)
4. Velocity of 92α line form Cesarsky and Cesarsky(1973)
5. Velocity of 1004 line from Viner et al(1979)

* Possible Carbon line

direction.

2. The line intensities are typically about 0.1 of the total continuum intensity and required integration times ranging from10 hours to 30 hours for detection with a signal to noise ratio between 5 and 10.

3. There is no marked difference in the line to total continuum intensity ratio between directions of HII regions, SNRs and blank regions.

4. Typical widths of the lines (FWHM) are 20-50km/s. However for many sources, particularly those in the longitude range 20 to 30 the lines are much wider (60-80km/s) or have more than one component for many sources and particularly so for those in the longitude range 20 to 30 . The line towards 3C391 is particularly narrow; the FWHM is only about 11km/s after correcion for instrumental broadening.

5. The strongest H272α line detected is towards the galactic centre. The profile clearly shows 3 components; one centered at 0 km/s, one around -50 km/s and the other at a positive velocity.

6. The H272α line towards the sources Orion A and Orion B (NGC 2024), are at negative velocities (-36km/s). High frequency recombination lines have been reported only at positive velocities ($\sim$10km/s).

7. Judging by the velocity shift with respect to the hydrogen line, carbon lines can be identified in about 12 cases. These lines are however somewhat wider than the carbon lines observed at higher frequencies, and have widths in the range of 20-30km/s.

5.6 COMPARISON WITH OTHER LOW FREQUENCY OBSERVATIONS :

Recombination lines from a few individual sources in this survey have been observed before, at frequencies below 500MHz, by other workers using other telescopes. For comparison we have selected all those sources common to the list given in Table 5.1, and observed elsewhere at frequencies closest to that of this survey. The frequency of observation, angular resolution, observed line parameters and references are given in Table 5.3. We can now compare these parameters with those given Table 5.2 for the corresponding sources. The observed line intensities and centroids are in good agreement for most of the sources. The slight differences in these quantities can be the result of the very different beam sizes in the two observations. The noticeable differences between the two sets of observations are the following.

The width of the line towards the SNR 3C391 observed at this frequency is much smaller than at higher frequencies. On the other hand, the lines towards SgrA and M17 are somewhat broader. The observations towards W51B at our frequency seem to show additonal components at higher velocities. But these components have to be treated with caution since the observations towards this source were affected by interference. Further, we have not detected any lines towards W51C and W51A, and our upper limits are somewhat lower than the intensities reported by Terzian and Pankonin (1974). Again, some of these differences are may be due to the different angular resolutions, frequencies and sensitivities of the two sets of observations.

5.7 BROAD IMPLICATIONS OF THE RESULTS :

A detailed interpretaion of the data presented in this chapter in terms of the distribution and properties of the gas responsible for the observed lines will be presented in subsequent chapters. In this section we indicate only the broad charecteristics of the data and their implications for the nature of the line emitting regions.

>

TABLE 5.3 :Parameters From Other Observations for comparison

Source	name	Freq MHz	Size (')	T_L/T_C x10^3	T_C °K	T_L °K	Width km/s	V_{LSR} km/s	Ref
G359.9-0.0	SGR A	328	50	1.5	1770	2.6(0.4)	26(5)	2.1(1.5)	1
G15.1-0.7	M17	386	35	1.0 1.1	527	0.5(0.2) 0.6(0.1)	24(17) 34(20)	15 51	2
G30.8-0.0	W43	328	50	2.4	380	0.9(0.4)	48(11)	102(10)	1
G31.9+0.0	3C391	428	11	2.5	466	1.15	63	90	3
G43.2+0.0	W49A	318	16	3.0	250	0.75(0.2)	25(8)	62(6)	4
G49.0-0.3	W51B	318	16	2.3	860	2.0(0.3)	25(9)	60(7)	4
G49.0-0.6	W51C	430	9	3.2(0.8)			15(4)	56(2)	5
G49.5-0.4	W51A	428	11	1.8(0.3)	530		31(7)	55(3)	6
G206.1-2.3	W16	386	36	3.8	89	0.34(0.12)	38(15)	16	2

References:

1. Pedlar et al (1978)
2. Gordon et al (1974)
3. Pankonin (1975)
4. Patrish et al (1977)
5. Terzian and Pankonin (1974)
6. Pankonin et al (1974)

5.7.1 Line Intensities

As discussed earliar, the recombination lines observed at this frequency can only sample conditions in relatively low density ionized regions. Macroscopic properties of a large selection of HII regions in the galactic plane have been studied by Shaver and Goss (1970b). Most of the HII regions common to the present 272α recombination line survey and the continuum survey of Shaver and Goss (1970b) have electron densities greater than 100cm^{-3} and sizes less than 10'. With these densities and sizes, effects of pressure broadening, optical depth and beam dilution make the recombination lines at this frequency virtually undetectable from these HII regions. The observed recombination lines must arise from much lower density gas having a much larger angular size. The gas can either be associated with the HII region, for example as an outer envelope or just lying along the line of sight. Further, the intensity and width of the recombination lines detected in this survey are very similar in all directions observed, irrespective of whether the direction corresponds to that of an HII region, an SNR or a blank region. The intensities of the lines are found to correlate well with the total continuum intensity. In the galactic plane where most of these observed sources lie, the continuum radiation at this frequency is mainly nonthermal in origin. Therefore, the line and continuum radiation originate in different regions along the line of sight. The HII regions and SNRs only add to the background continuum radiation, and the lines themselves must arise in low density ionized regions along the line of sight. The ORT beam of 2°x6' and the low observing frequency are probably well suited for studying the properties of such low density ionized gas not prominent in the continuum At higher frequencies, where better angular resolutions are available and where the expected intensity of recombination lines from the HII regions themselves are much higher, it would be difficult to separate out the two contributions.

5.7.2 Stimulated Emission

Stimulated emission of recombination lines due to non-LTE populations of high principal quantum number levels is expected to be important at low frequencies (Shaver 1975). Presence of a strong background source or even the non-thermal galactic background is expected to have considerable influence on the line intensities. Pedlar et al (1980) have demonstrated that the intensity of the low frequency recombination line towards the galactic centre is enhanced by the background continuum sources in that direction. In figure 5.8 we have plotted the peak line brightness temperature T_{BL}, observed in different directions, against the total continuum temperature T_{BS} which includes the non thermal galactic background. There is a good correlation between T_{BL} and T_{BS} (correlation coefficient = 0.78) indicating that the line intensities are enhanced by the background radiation. In particular, if this were not the case, the observed line to continuum ratio should have been much higher for sources in the anticentre direction, where the non-thermal galactic background is much less. It may be noted here that such a correlation between line and continuum intensity has been observed even at 5GHz (Jackson and Kerr 1975). But at this frequency the continuum is mainly thermal, and the correlation is expected even in the absence of stimulated emission. However at low frequencies (<500MHz) the continuum intensity is dominated by the non-thermal emission and any correlation between T_{BL} and T_{BS} can only be due to stimulated emission

5.7.3 The Line Velocities

The radial velocities of the ionized region responsible for the recombination line are indicated by the observed frequency of the line centre. This velocity with resepct to LSR for all the observed lines is given in column 4 of Table 5.2. The measured radial velocity of an object in the galactic plane is an indicator of its location along the line of sight.

It is useful to compare the velocity of the H272α line

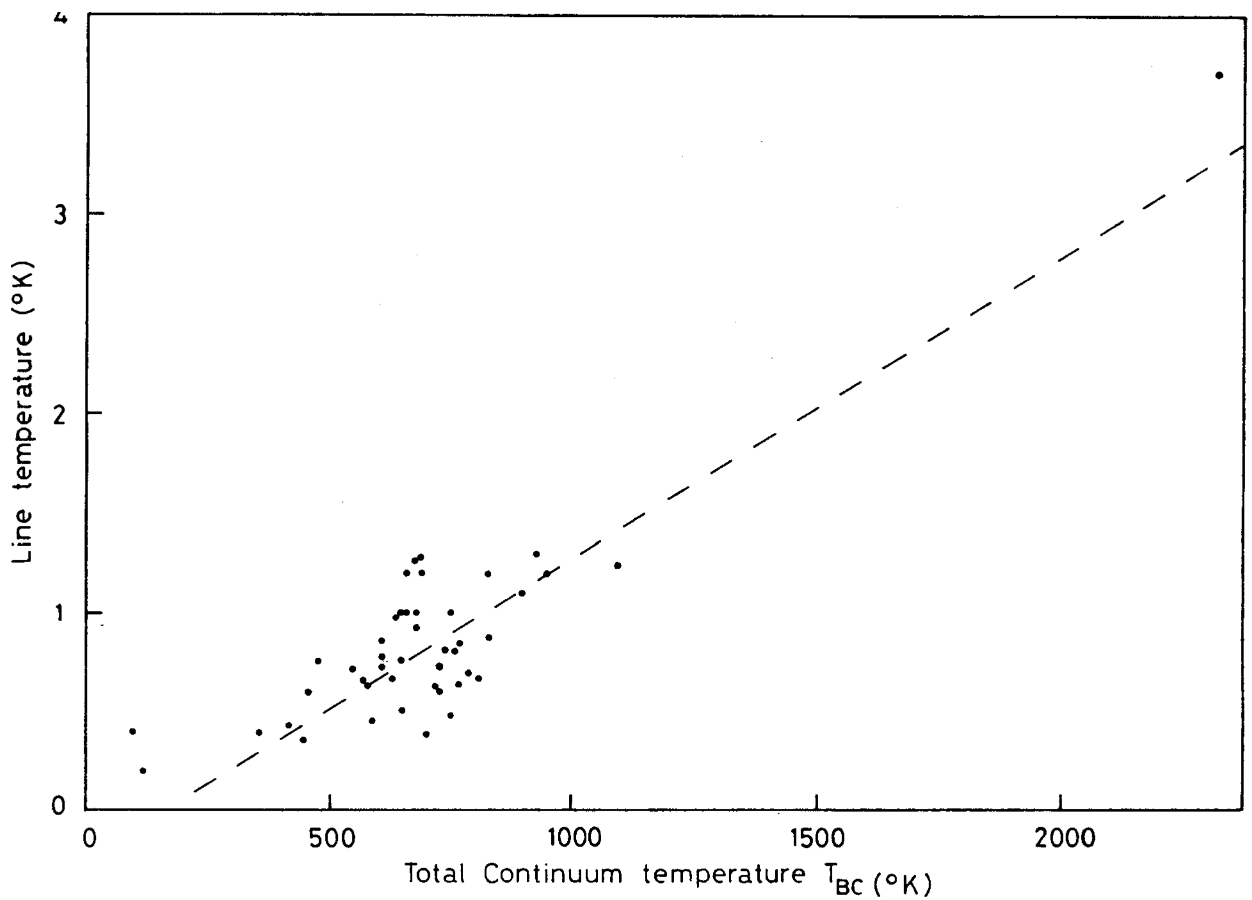

Fig. 5.8 Observed H272α peak line intensity as a function of T_{BC}.

observed here with that of a higher frequency recombination line, as the latter arises preferentially in the relatively high density HII regions along the line of sight. Column 9 of Table 5.2 gives the velocity of H110α (~5GHz) observed by Downes et al (1980) towards the same directions. Column 10 is the difference between the observed H272α velocity and the H110α velocity. A histogram of these differences is shown in figure 5.9. These differences will indicate the separation along the line of sight between the HII regions from which the H110α line is observed and the lower density gas from which H272α line is observed. If the two lines arise from closely associated regions, then this difference in velocity would be very small. The histogram in fig 5.8 shows that in 60% of the cases the velocity difference is within 10km/s. As these differences are small compared to the width of the lines (20-50km/s), they suggest a physical association between the regions emitting the high frequency and the low frequency recombination lines. However in those cases where the differences are large, the two regions have to be physically widely separated, unless there is differential motion between the higher and lower density regions.

5.7.4 The l-v Diagram

The longitude-velocity diagram of the lines observed is an indicator of the distribution of the gas responsible for the lines in the galactic disk. Figure 5.10 is the l-v diagram of the H272α lines observed in this survey. This can be compared with l-v diagram for the 21 cm HI emission in the galactic plane (see chapter 7). It is clear that the gas responsible for the low frequency recombination line is not distributed like the neutral hydrogen. The HI emission occupies a much larger velocity range in such a diagram (see chapter 7). This rules out the possibility that the line emitting regions are partially ionized neutral hydrogen clouds. Ionization in cold HI clouds may not be adequate to produce detectable recombination lines at this frequency. Further, the width of these lines, which is in the range of 20-50km/s, indicates that these lines do not arise from a distributed component of the interstellar medium

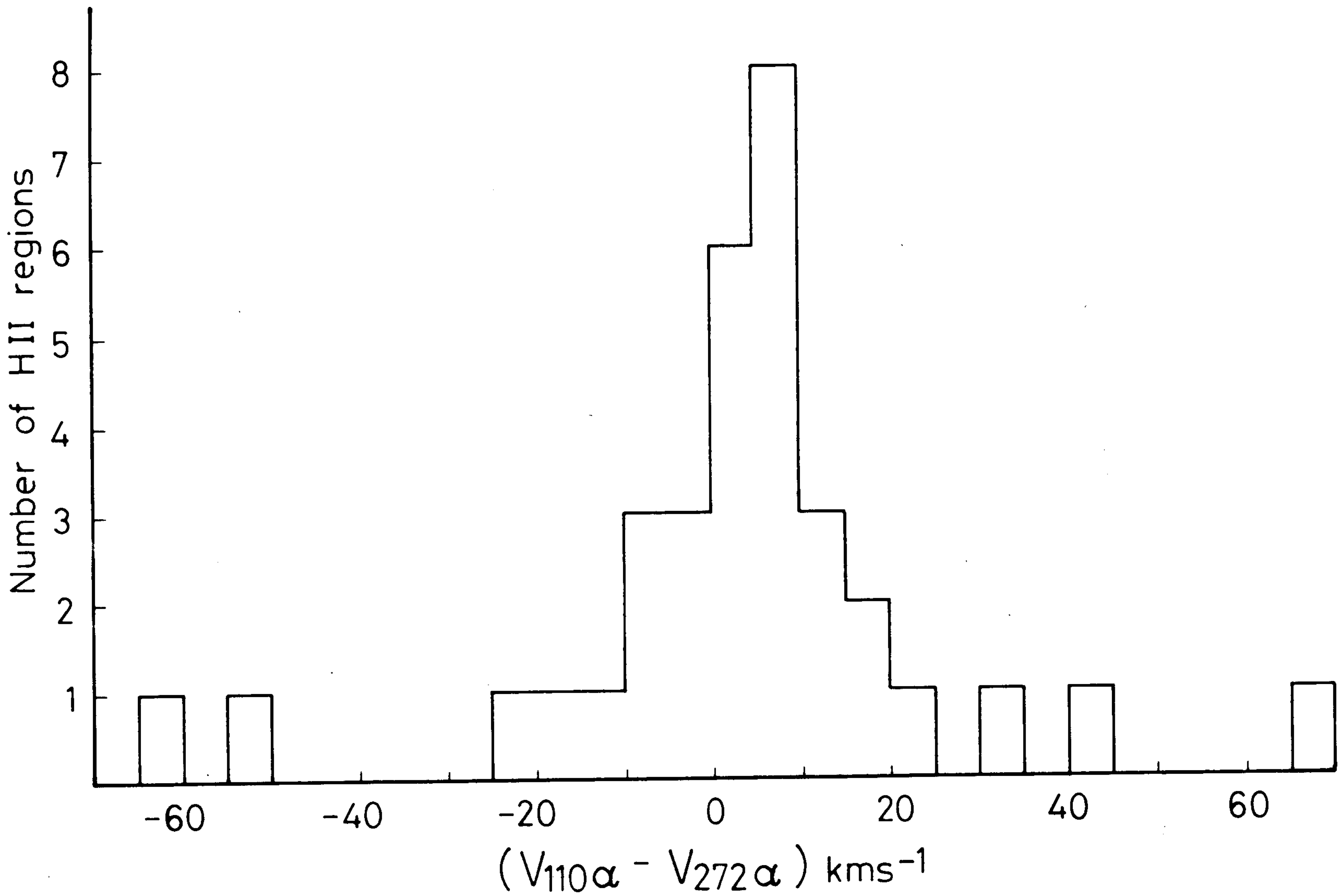

Fig. 5.9 Histogram of the velocity differences between H110α lines (see table 5.2) and the observed H272α lines.

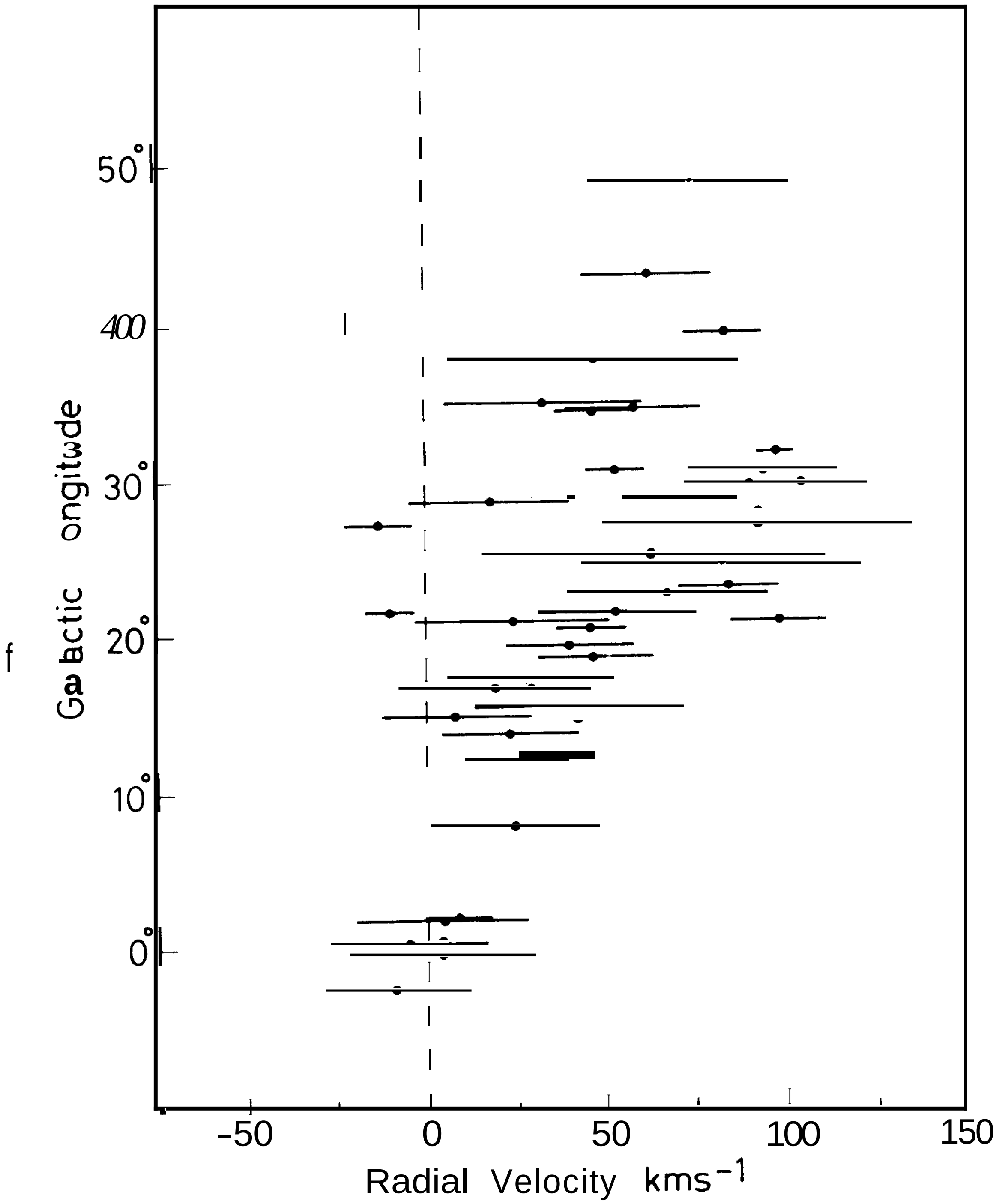

Fig. 5.10 l-v diagram for the observed H272α lines. The dot indicates the central velocity and the horizontal line represents the half power width.

On the other hand the l-v diagram in fig 5.10 is similar to those of HII regions seen in an H110α survey (see Wilson 1980), the ionized galactic ridge seen in an H166α survey (Lockman 1980), and molecular clouds seen in the CO surveys (see Sanders 1983). The distributions of both HII regions and molecular clouds in the galactic disk show a peak between 4 kpc and 8 kpc from the galactic centre (Wilson 1980 Sanders 1983). While most of the recombination lines observed here do not arise in the HII regions seen in the H110α survey, for reasons discussed earlier, the l-v diagram in fig 5.10 indicates that the low density gas responsible for these lines is distributed in a manner similar to HII regions and molecular clouds in the inner part of the galaxy. As the H272α recombination line is detected in every direction observed for $l < 40^{\circ}$ representetive quantities of low density ionized gas must be present in every direction in this range.